

The Nucleocapsid Protein of SARS-CoV-2 Abolished Pluripotency in Human Induced Pluripotent Stem Cells

1 **Zebin Lin^{1,2#}, Zhiming Wu^{3#}, Jinlian Mai², Lishi Zhou², Yu Qian¹, Tian Cai⁴, Zhenhua Chen⁴,**
2 **Ping Wang^{5*} and Bin Lin^{2*}**

3 ¹School of Pharmaceutical Sciences, Sun Yat-Sen University, Guangzhou, China

4 ²Guangdong Beating Origin Regenerative Medicine Co. Ltd., Foshan, China

5 ³Department of Urology, Sun Yat-sen University Cancer Center, State Key Laboratory of Oncology
6 in South China, Collaborative Innovation Center for Cancer Medicine, Guangzhou, China

7 ⁴Nanhai District People's Hospital of Foshan, Foshan, China

8 ⁵School of Medical Imaging, Tianjin Medical University, Tianjin, China

9 [#]These authors contributed equally to the work.

10 *** Correspondence:**

11 Ping Wang

12 pingwang@tmu.edu.cn;

13 Bin Lin

14 linbin@beatingorigin.com.

15

16 **Keywords:** SARS-CoV-2, nucleocapsid protein, human induced pluripotent stem cell,
17 pluripotency, fibroblast.

18

19

20

21

22

23

24

25

26

27

28 Abstract

29 The COVID-19 pandemic caused by severe acute respiratory syndrome coronavirus 2 (SARS-CoV-
30 2) is raging across the world, leading to a global mortality rate of 3.4% (estimated by World Health
31 Organization in March 2020). As a potential vaccine and therapeutic target, the nucleocapsid protein
32 of SARS-CoV-2 (nCoVn) functions in packaging the viral genome and viral self-assembly. To
33 investigate the biological effects of nCoVn to human stem cells, genetically engineered human
34 induced pluripotent stem cells (iPSC) expressing nCoVn (iPSC-nCoVn) were generated by
35 lentiviral expression systems, in which the expression of nCoVn could be induced by the
36 doxycycline. The proliferation rate of iPSC-nCoVn was decreased. Unexpectedly, the morphology
37 of iPSC started to change after nCoVn expression for 7 days. The pluripotency marker TRA-1-81
38 were not detectable in iPSC-nCoVn after a four-day induction. Meanwhile, iPSC-nCoVn lost the
39 ability for differentiation into cardiomyocytes with a routine differentiation protocol. The RNA-seq
40 data of iPSC-nCoVn (induction for 30 days) and immunofluorescence assays illustrated that iPSC-
41 nCoVn were turning to fibroblast-like cells. Our data suggested that nCoVn disrupted the
42 pluripotent properties of iPSC and turned them into other types of cells, which provided a new
43 insight to the pathogenic mechanism of SARS-CoV-2.

44 1 Introduction

45 Right now, the COVID-19 pandemic is sweeping the world, causing a huge crisis in public health
46 and economics globally. According to the continuously updated data from World Health
47 Organization, to date, nearly three million infected cases were confirmed, while more than 200,000
48 individuals died because of COVID-19 (<https://www.who.int/emergencies/diseases/novel-coronavirus-2019>). Severe acute respiratory syndrome coronavirus 2 (SARS-CoV-2), which was
49 proved to be the pathogen of COVID-19, has 79% identity in genomes with severe acute respiratory
50 syndrome coronavirus (SARS-CoV) (Lu et al., 2020). Twelve coding regions were predicted in
51 SARS-CoV-2, including spike protein, nucleocapsid protein, envelope protein, and membrane
52 protein (Lu et al., 2020; Wu et al., 2020; Xu et al., 2020). The Cryo-EM structure of spike protein
53 had been determined (Wrapp et al., 2020), and more and more evidences showed that the spike
54 protein binds human ACE2 to entry into host cells (Hoffmann et al., 2020; Wrapp et al., 2020), which
55 indicated that SARS-CoV-2 might share similar pathogenic mechanisms with SARS-CoV. Because
56 of the very limited knowledge of SARS-CoV-2, we sought to understand the biology of SARS-CoV-
57 2 based on the previous studies about SARS-CoV.

58 As one of the most studied proteins in SARS-CoV, the nucleocapsid protein binds to viral RNA to
59 package the genome in a ribonucleoprotein particle (Chang et al., 2014). Unlike the spike protein
60 with a certain mutation frequency, the sequence of nucleocapsid protein was more stable (Chinese,
61 2004), which meant it was an ideal target for diagnostic tools (Severance et al., 2008; Suresh et al.,
62 2008; Das et al., 2010) and antiviral therapy (Cheung et al., 2008; Chang et al., 2016). The
63 pathogenic effects in host cells caused by the nucleocapsid protein were also studied. It was reported
64 that the nucleocapsid protein inhibited type I interferon production after virion infected the host cells
65 (Hu et al., 2017), which was considered as a possible mechanism of immune escape. The
66 nucleocapsid protein inhibited cell cytokinesis and proliferation (Zhou et al., 2008), and regulated
67 several pathways, such as transforming growth factor-beta signaling (Zhao et al., 2008), AP-1 signal
68 transduction pathway (He et al., 2003), and NF-KappaB pathway (Zhang et al., 2007b). Besides, the
69 nucleocapsid protein was reported as an apoptosis inducer in COS-1 cells (Surjit et al., 2004; Zhang
70 et al., 2007a) and HPF cells (Zhao et al., 2006).

72 As the nucleocapsid protein of SARS-CoV-2 (nCoVN) has 88.1% identity with the nucleocapsid
73 protein of SARS-CoV (Lu et al., 2020), it is reasonable to speculate that they share a same
74 pathogenic pathway in host cells. The original goal of this study is to determine the physiological
75 malfunctions, such as cardiac fibrosis, in human cardiomyocytes expressing nCoVN by using human
76 induced pluripotent stem cells (iPSC) and direct cardiac-differentiation methods. However, the
77 morphology of iPSC altered obviously when nCoVN had been expressed for 7 days. This unexpected
78 observation inspired us some new thoughts: (i) It was likely that the adult stem cells could be
79 infected by SARS-CoV-2, in spite of lacking of the clinical data; (ii) iPSC were appropriate study
80 materials for stem cell research because of avoiding many ethical issues; (iii) The preliminary data
81 indicated that nCoVN seemed to be deleterious to iPSC, which meant it might also cause damages in
82 other stem cells. Therefore, we turned to investigate whether nCoVN obstructed the pluripotency
83 maintenance in iPSC. We believed that this study could help us to understand the deleterious effects
84 of nCoVN to human adult stem cells and embryonic stem cells.

85 2 Method

86 2.1 Cell culture and differentiation assay

87 Human induced pluripotent stem cells (iPSC) DYR0100 (from The American Type Culture
88 Collection, ATCC) were plated on Matrigel matrix (hESC-Qualified, LDEV-Free, Corning, 354277)-
89 coated plates, and then were cultured in DMEM/F-12 medium (Gibco, 11320033) supplemented with
90 STEMUP® ES/iPS cell culture medium supplement (Nissan Chemical Corporation). STEMUP
91 medium was changed every two days. iPSC were passaged every three to four days or when the cell
92 culture was 80-90% confluent. During passages, iPSC were rinsed with 1× DPBS (Gibco, 14040133)
93 for one time then were treated with 0.5 mM EDTA (Invitrogen, 15575020) in 1× DPBS (Gibco,
94 14190144) for 10 minutes at room temperature. The split ratio was 1:3-1:6. The detailed
95 differentiation protocol was described in the previous published reports (Lin et al., 2017; Shekhar et
96 al., 2018). Briefly, iPSC were treated with the small molecule CHIR99021 (Tocris, 4423, final
97 concentration 10 µM) in the RPMI-BSA medium [RPMI 1640 Medium (HyClone, SH30027.01)
98 supplemented with 213 µg/ml AA2P (l-ascorbic acid 2-phosphate magnesium) (Sigma, A8960) and
99 0.1% bovine serum albumin (BSA) (Sigma, A1470)] for 24 hours, then were incubated with RPMI-
100 BSA medium for 48 hours. On differentiation day 4, cells were treated with the small molecule IWP2
101 (Tocris, 3533, final concentration 5 µM) in RPMI-BSA medium. After 48 hours, the medium was
102 changed to RPMI-BSA medium. Then, RPMI 1640 medium supplemented with 3% KnockOut
103 Serum Replacement (Gibco, 10828-028) was used to culture the cardiomyocytes in the following
104 experiments. All the cells in this study (except iPSC-derived cardiomyocytes) were kept culturing in
105 the STEMUP medium until they were applied to other assays.

106 2.2 Generation of iPSC-nCoVN

107 The cDNA of nCoVN with a N-terminal 6× His Tag coding sequence (GeneMedi) and puromycin
108 resistance gene were sub-cloned into the plasmid pCW-Cas9-Blast (Addgene, 83481) to replace Cas9
109 and Blast cDNA, respectively. Lentivirus preparation using a third generation lentivirus packaging
110 system were referred to the previous report (Jiang et al., 2015). We followed and modified the
111 protocol from Zhang lab to detect MOI of the lentivirus and perform transduction (Shalem et al.,
112 2014). After 24 hours of transduction, medium was changed to fresh STEMUP medium
113 supplemented with doxycycline hyclate (Sigma, D9891) for induction. Two days later, puromycin
114 (InvivoGen, ant-pr-1, final concentration 2 µg/mL) was added into the STEMUP medium
115 supplemented with doxycycline hyclate. After 2-3 days' selection, which resulted in a transduction
116 efficiency of ~30%, single cell clones were manually picked and re-seeded in separated wells. For

117 nCoVN expression induction, doxycycline hyolate (Sigma, D9891) was supplemented in the stem
118 cell culture medium at a final concentration of 2 μ g/mL, and the same amount of DMSO was added
119 to the stem cell culture medium for controls.

120 **2.3 Reverse transcription-PCR and Quantitative Real-time PCR**

121 Total RNA was extracted by using the UNIQ-10 Column Trizol Total RNA Isolation Kit (Sangon
122 Biotech, B511321-0100) prior to the treatment with DNase I (Sangon Biotech, B618252) for 30
123 minutes. mRNA was reverse transcribed by using iScript Reverse Transcription Supermix (Bio-Rad,
124 1708841). Quantitative Real-time PCR was performed by using a PikoReal Real-Time PCR
125 System (Thermo Fisher) with SsoAdvancedTM Universal SYBR[®] Green Supermix (Bio-Rad,
126 1725271). The primers for Reverse transcription-PCR and Quantitative Real-time PCR are as
127 followed (from 5' to 3'):

128 ACE2-RT-F: GGTCTTCTGTCACCCGATT;

129 ACE2-RT-R: ACCACCCCAACTATCTCTCG;

130 nCoVN-RT-F: CATTGGCATGGAAGTCACAC;

131 nCoVN-RT-R: TCTGCGGTAAGGCTTGAGTT;

132 GAPDH-RT-F: TGGGTGTGAACCATGAGAAG;

133 GAPDH-RT-R: GTGTCGCTGTTGAAGTCAGA.

134 **2.4 The proliferation assay**

135 iPSC, iPSC-GFP and iPSC-nCoVN were seeded in 96-well plates with the same cell number. After
136 24 hours, CCK-8 reagent was added in the medium to monitor the proliferation rate (Beyotime,
137 C0038). The absorbance at 450 nm was measured at 24 hours, 42 hours, 48 hours, 60 hours and 72
138 hours by using Varioskan Flash Multimode Reader (Thermo Scientific). The cell-free medium with
139 CCK-8 reagent were used as blank control sets. The data were analyzed and plotted using GraphPad
140 Prism 6.

141 **2.5 Immunofluorescence Staining**

142 Cells were fixed with 4% paraformaldehyde at room temperature for 20 minutes and washed three
143 times with 1 \times PBS. Cells were then permeabilized with PBS containing 0.25% Triton X-100 at room
144 temperature for 10 minutes. After incubating in the blocking buffer (1 \times PBS with 10% goat serum),
145 cells were stained with different primary antibodies at 4°C overnight. These primary antibodies were
146 [target, dilution, species, company, product number]: Troponin T Cardiac Isoform, 1:100, mouse,
147 Thermo Fisher, MA5-12960; alpha-smooth muscle actin, 1:100, mouse, Bioss, bsm-33187M;
148 S100A4, 1:100, rabbit, Bioss, bs-3759R; SSEA4, 1:250, mouse, Invitrogen, 14-8843-80; TRA-1-81,
149 1:250, mouse, Invitrogen, 14-8883-80; 6 \times His Tag, 1:250, mouse, Sangon Biotech, D191001; OCT4,
150 1:200, mouse, Abcam, ab184665; ACE2, 1:200, rabbit, Bioss, bs-1004R; vimentin, 1:250, rabbit,
151 Bioss, bs-0756R. Cells were washed three times with PBS containing 0.1% Triton X-100, then
152 incubated with the Alexa Fluor 488 goat anti-mouse or Alexa Fluor 555 goat anti-rabbit IgG
153 secondary antibodies at 37°C for 1 hour. Nuclei were labeled with DAPI (4',6-diamidino-2-
154 phenylindole, 1 μ g/ml) for 5 minutes. Images were obtained by using the DMi6000 B inverted

155 microscope (Leica) or the FV1000 confocal laser scanning microscope (Olympus), then were
156 analyzed by using ImageJ software.

157 **2.6 RNA-seq analysis method**

158 RNA-seq was performed by Novogene Co., Ltd. We obtained 151 bp paired-end RNA-seq reads
159 from an Illumina Novaseq instrument, average 23 million read pairs for 3 iPSC-GFP and 3 iPSC-
160 nCoVN samples. Adapters and low-quality bases in reads were trimmed by trim_galore (v0.6.5;
161 http://www.bioinformatics.babraham.ac.uk/projects/trim_galore/). We employed Kallisto (v0.46.0)
162 (Bray et al., 2016) to determine the read count for each transcript and quantified transcript abundance
163 as transcripts per kilobase per million reads mapped (TPM), using gene annotation in the GENCODE
164 database (v32, GRCh38) (Frankish et al., 2019). Then we summed the read counts and TPM of all
165 alternative splicing transcripts of a gene to obtain gene expression levels. We restricted our analysis
166 to 22,201 expressed genes with an average TPM ≥ 1 in either iPSC-GFP or iPSC-nCoVN samples.
167 DESeq2 (v1.26.0) (Love et al., 2014) was used to identify differentially expressed genes (DEGs)
168 (false discovery rate (FDR) < 0.05 and $\text{abs}(\text{log2FoldChange}) > 3$). The pathway analysis was
169 performed by ToppGene Suite (Chen et al., 2009). The raw RNA-seq data have been deposited in
170 GEO, and the accession number is pending.

171 We took gene expression values (i.e. $\log_2(\text{TPM})$) in iPSC/ESC and fibroblast from ENCODE
172 (Consortium, 2012; Davis et al., 2018). Combining with our RNA-seq data, quantile normalization
173 (Bolstad et al., 2003) was performed, and then ComBat (Johnson et al., 2007) was used to remove the
174 batch correction. We selected the top 1000 genes with the largest variance to calculate the correlation
175 coefficients between samples. The heatmap was generated by pheatmap function in R.

176 **2.7 Statistic**

177 Values were expressed as mean \pm SD (standard deviation). Statistical significances were evaluated
178 using one-way ANOVA with Bonferroni correction or Student's T-Test. $P < 0.05$ was considered
179 statistically significant.

180 **3 Results**

181 **3.1 ACE2 was expressed in various of stem cells**

182 As ACE2 was the major receptor of SARS-CoV-2 on the cell membrane (Hoffmann et al., 2020;
183 Wrapp et al., 2020), we first examined whether ACE2 was expressed in the stem cells. Thanks to the
184 gene expression data collection in Gene Expression Omnibus (GEO,
185 <https://www.ncbi.nlm.nih.gov/geo/>), it was convenient to analyze the ACE2 expression profiles in
186 sorts of stem cells. Figure 1A showed the ACE2 expression values in different stem cells from
187 different projects, including human embryonic stem cells (Kim et al., 2014), iPSC (Yang et al.,
188 2014), human epithelial stem cells (Yang et al., 2014), human adipose stem cells (Onate et al., 2013),
189 human hematopoietic stem cells (Pang et al., 2011), and human mesenchymal stem cells (Bernstein
190 et al., 2010). The expression values of a housekeeping gene GAPDH were simultaneously collected
191 as controls. ACE2 was expressed in each kind of stem cells, though the expression values were
192 relatively low compared with GAPDH. The reverse transcription-PCR (RT-PCR) results showed that
193 ACE2 was expressed in iPSC, iPSC-derived cardiomyocytes (iPSC-CM) and human coronary artery
194 endothelial cells (HCAEC) (Figure 1B). The images from immunofluorescence assays clearly
195 showed that ACE2 protein was located on the cell membrane of iPSC (Figure 1C), suggesting that
196 the pluripotent stem cells were the potential targets of SARS-CoV-2.

197 **3.2 Expression of nCoVN changed the morphology of iPSC**

198 To study whether physiological activities in iPSC were disturbed by nCoVN, a human induced
199 pluripotent stem cell line (iPSC-nCoVN) in which the expression of nCoVN could be modulated by a
200 Tet-On system was generated by a lentiviral expression system. In this system, nCoVN cDNA
201 sequence (with a 6× His Tag coding sequence) was conjugated to puromycin resistance gene through
202 a T2A peptide encoding sequence, and the transcription was relied on the induction of tetracycline or
203 doxycycline (Dox). After puromycin selection, two single cell clones were seeded in separated wells
204 by manual colony-picking. Sequentially, iPSC-nCoVN were divided into two groups: one was
205 induced by Dox for nCoVN expression (Dox), the other was added with DMSO as a control set
206 (DMSO), meanwhile, a GFP-expressed iPS cell line (iPSC-GFP), in which the expression of GFP
207 was modulated by the same Tet-On system, was used as another control set in the following assays
208 (Figure 2A).

209 The expression of nCoVN was confirmed at the mRNA and protein levels. The transcriptional level
210 of nCoVN was measured by Real-time PCR in iPSC, Dox, and DMSO groups, and nCoVN
211 expression increased about 267-fold in the Dox group compared with the DMSO group (Figure 2B).
212 The nCoVN protein was detected by using an anti-6× His Tag antibody in cells from the Dox group
213 (Supplementary Figure 1). The proliferation rate was compared among iPSC, iPSC-GFP and Dox
214 groups by using a cell counting kit. The absorbance at 450 nm (A450) was measured at 24 hours, 42
215 hours, 48 hours, 60 hours and 72 hours after cell seeding. After three days of cell seeding, Dox group
216 showed a decreased proliferation rate than both of iPSC and iPSC-GFP groups, indicating that
217 nCoVN might hamper the growth and division of iPSC (Figure 2C). This observation was consistent
218 with the previous finding about the nucleocapsid protein of SARS-CoV (Zhou et al., 2008).

219 We continued to induce nCoVN expression in iPSC. The phase-contrast images of iPSC-nCoVN
220 with a 7-day, a 9-day, and an 11-day inductions (Dox) and counterpart controls (DMSO) were shown
221 in Figure 2D. In the DMSO group, a typical morphology of stem cells with high nucleus/cytoplasm
222 ratio and close cell membrane contacts was observed, while iPSC-nCoVN after a 7-day induction
223 started to exhibit endothelial cell morphological features and lower nucleus/cytoplasm ratio. After a
224 14-day induction, most of the cells exhibited distinct shapes from wild-type iPSC, such as neuron-
225 like cells, endothelial-like cells and fibroblast-like cells (Figure 2E). These data showed that
226 continuous expression of nCoVN caused obvious morphological changes in iPSC.

227 **3.3 Expression of nCoVN disabled the pluripotent properties of iPSC**

228 Next, we examined the pluripotency markers in iPSC and iPSC-nCoVN. The pluripotency markers
229 SSEA4 and TRA-1-81, which were expressed in human embryonic stem cells and iPSC, were widely
230 applied in identification of pluripotent stem cells (Abujarour et al., 2013; Trusler et al., 2018). The
231 immunofluorescence staining images illustrated that iPSC-nCoVN completely lost the expression of
232 SSEA4 and TRA-1-81, namely, iPSC-nCoVN lost the pluripotency in the presence of nCoVN
233 (Supplementary Figure 2A, B). We traced the expression of TRA-1-81 in iPSC-nCoVN with a 2-day,
234 a 4-day, a 6-day, and an 8-day inductions (Figure 3A). On Day 2, TRA-1-81 was still expressed in
235 iPSC-nCoVN; however, from Day 4, TRA-1-81 was not detectable in most of the cells, suggesting
236 that the pluripotent fate of iPSC-nCoVN was determined in the first 4 days. To further test the
237 pluripotency in iPSC and iPSC-nCoVN, we directly differentiated these cells to cardiomyocytes by
238 using a routine protocol, and the differentiation assays were performed under the same conditions. As
239 expected, the differentiation efficiency could reach 60% in iPSC; however, on differentiation day 12,
240 only a very small portion of cells from iPSC-nCoVN were expressed cardiac Troponin T,

241 accompanied by many cell deaths (Figure 3B, C). This differentiation assay provided solid evidence
242 that the pluripotency maintenance of iPSC-nCoVN was disrupted by nCoVN.

243 **3.4 Long-term expression of nCoVN drove iPSC to fibroblast**

244 Since the pluripotency lost due to short-term expression of nCoVN, we are extremely interested in
245 the cell fate of iPSC-nCoVN under long-term expression of nCoVN. After a 28-day induction in the
246 stem cell culture medium, some spindle-shaped iPSC-nCoVN, which exhibited a typical fibroblast
247 morphological feature, were observed (Supplementary Figure 2C). The antibodies against fibroblast
248 markers vimentin, alpha-smooth muscle actin (α -SMA) and S100A4 were used to verify the cell type
249 of these fibroblast-like cells. The results from immunofluorescence assays confirmed that these
250 markers were expressed in nCoVN-expressing cells (Figure 4A, B, C; Supplementary Figure 2D). To
251 further investigate the transcriptomic profiles of iPSC-nCoVN under the long-term nCoVN
252 expression, doxycycline-induced iPSC-nCoVN and iPSC-GFP for 30 days were applied to RNA-seq.
253 Through differentially express analysis, iPSC-nCoVN showed a dramatic gene expression change
254 comparing with iPSC-GFP (Supplementary Table). Totally, 3,080 genes were significantly
255 differentially expressed ($FDR < 0.05$, $|\log_2 \text{FoldChange}| > 3$). Among them, the down-regulated genes
256 in iPSC-nCoVN were most significantly enriched with proliferation and stem cell related pathways,
257 including the Yamanaka factors-associated genes, such as *POU5F1*, *LIN28A*, *NANOG*, and *SOX2*
258 (with a 790-fold, a 2306-fold, a 253-fold, and an 18-fold decrease, respectively) (Figure 4E); while
259 the extracellular matrix and extracellular matrix-associated pathway was the most significantly
260 enriched pathway in the up-regulated genes (Figure 4F). Next, we used RNA-seq data from the
261 ENCODE project to evaluate the cell type of iPSC-nCoVN. Comparing with the transcriptome of the
262 pluripotent stem cells and fibroblast in the ENCODE project (Consortium, 2012; Davis et al., 2018),
263 iPSC-GFP samples were clustered with H7 and GM23338, which were the embryonic stem cells
264 (ESC) and iPSC, respectively; while iPSC-nCoVN samples were clustered with multiple kinds of
265 fibroblast (Figure 4G). Furthermore, iPSC-nCoVN with a 40-day induction, which were kept
266 culturing in the stem cell medium, were totally differentiated to fibroblast (Figure 4D).

267 **4 Discussion**

268 According to the current knowledge about the life cycle of SARS-CoV, the nucleocapsid protein was
269 translated by the host cell translation protein synthesis machinery (McBride et al., 2014; Song et al.,
270 2019), and was localized mainly in the cytoplasm (Rowland et al., 2005). The primary function of
271 nucleocapsid protein was to package the viral genome into nucleocapsids to protect the genomic
272 RNA (McBride et al., 2014). During the formation of nucleocapsids, numerous nucleocapsid proteins
273 bound to the viral RNA and started oligomerization. The viral reproductive strategies would
274 synthesize nucleocapsid proteins as many as possible to meet the requirements of viral assembly,
275 which meant the nucleocapsid proteins were overproduced. The findings that redundant nucleocapsid
276 proteins interfered with the normal physiology of host cells were reported (Surjit et al., 2004; Zhao et
277 al., 2006; Zhang et al., 2007a; Zhao et al., 2008; Zhou et al., 2008; Hu et al., 2017). In this study, we
278 first presented that nCoVN abolished pluripotency and reduced the proliferation rate in human
279 induced pluripotent stem cells. Long-term expression of nCoVN drove iPSC to fibroblast
280 in spite of using the stem cell culture conditions. It was reported that the nucleocapsid protein of
281 SARS-CoV facilitated TGF- β -induced PAI-1 expression to promote lung fibrosis (Zhao et al., 2008),
282 which was also the possible pathway that nCoVN turned iPSC to fibroblast.

283 The time-course assays showed that the pluripotency marker disappeared in four days after nCoVN
284 expression. This finding might be applied to a cell-based chemical screening model, in which the

285 candidate chemicals with potential ability to halt the iPSC differentiation caused by nCoVN are
286 easily identified. More importantly, SARS-CoV-2 is not necessary in this model, which means it
287 could be used in the routine laboratories and applied to high-throughput equipment with less risk.

288 In addition, how nCoVN breaks the pluripotency maintenance of iPSC is still a riddle. The
289 pluripotency maintenance in stem cells requires delicate regulations to maintain the balance of
290 pluripotency gene expression in a complicated network. Since nCoVN can bind RNAs, it is possible
291 that nCoVN suppresses the key pluripotency gene's translation through occupying the particular sites
292 of RNAs. Although the mechanism is unknown, the toxic effects of nCoVN are clear, which reminds
293 us that SARS-CoV-2 might impair the reproductive system and hematopoietic system. In conclusion,
294 we first reported expressing nCoVN could totally change the cell fate of iPSC, which provided new
295 clues to help people fighting against the virus.

296 5 Conflict of Interest

297 *Author Zebin Lin, Jinlian Mai, Lishi Zhou, and Bin Lin were employed by the company Guangdong
298 Beating Origin Regenerative Medicine Co. Ltd. The remaining authors declare that the research was
299 conducted in the absence of any commercial or financial relationships that could be construed as a
300 potential conflict of interest.*

301 6 Author Contributions

302 ZL, ZW, PW, and BL had substantial contributions to the design of the paper; ZL, ZW, JM, LZ, YQ,
303 and TC performed the experiments and analysed the data; ZC provided critical suggestions to
304 improve the paper; ZL, ZW, PW, and BL wrote the manuscript. All authors (ZL, ZW, JM, LZ, YQ,
305 TC, ZC, PW, and BL) had read and approved the final manuscript.

306 7 Funding

307 This work was supported by grants from the National Natural Science Foundation of China (NSFC)
308 to Ping Wang (31900812).

309 8 Acknowledgments

310 This work is dedicated to all the medical staff who are still fighting against COVID-19 in China.
311 Your efforts make us safer.

312 9 Figure legends

313 **Figure 1.** ACE2 was expressed in human stem cells. (A) Expression values of ACE2 and GAPDH
314 derived from the Gene Expression Omnibus database. (B) Images from agarose gel electrophoresis
315 for analyzing the Reverse transcription-PCR products. ACE2 was expressed in iPSC, iPSC-CM and
316 HCAEC. iPSC, human induced pluripotent stem cell; iPSC-CM, human induced pluripotent stem
317 cell-derived cardiomyocyte; HCAEC, human coronary artery endothelial cell; NC, negative control.
318 (C) Representative immunofluorescent staining images of ACE2 (red) and the pluripotency marker
319 OCT4 (green) in iPSC. The cell nuclei were stained by DAPI (blue). The scale bar represents 10 μ m.

320 **Figure 2.** nCoVN affected the proliferation and morphology of iPSC. (A) Schematic diagram
321 illustrating the generation of iPSC-nCoVN and controls. Purple cells indicated iPSC without nCoVN
322 expression, while yellow cells indicated iPSC with nCoVN expression. Green cells were iPSC stably

323 expressing GFP under the doxycycline induction. (B) The mRNA expression level of nCoVN was
324 significantly elevated in iPSC-nCoVN for a long-term induction (n=3). **, $p<0.001$. (C) The time
325 course of cellular proliferation from iPSC, iPSC-GFP and iPSC-nCoVN (n=6). At 72 hours after cell
326 seeding, the values of A450 were significantly increased in iPSC and iPSC-GFP groups. **, $p<0.001$.
327 (D) Representative phase-contrast images from nCoVN-positive cells (Dox group) and control cells
328 (DMSO group) after a 7-day, a 9-day, and an 11-day inductions. The scale bar is 50 μ m. (E)
329 Representative phase-contrast images of iPSC-nCoVN after a 14-day induction show detailed
330 morphological alterations. Images were taken under objectives with 10 \times , 20 \times , and 40 \times
331 magnifications (from left to right panels). White dashed line boxes indicate the regions that are
332 magnified in the right panel. The scale bar represents 50 μ m.

333 **Figure 3.** iPSC-nCoVN lost the pluripotency. (A) Representative immunofluorescent staining images
334 of pluripotency marker TRA-1-81 (green) in iPSC-nCoVN for a 2-day, a 4-day, a 6-day, and an 8-
335 day inductions. The cell nuclei were stained by DAPI (blue). The scale bar represents 50 μ m. (B)
336 Representative immunofluorescent staining images of cardiomyocyte marker cardiac Troponin T
337 (Red) in iPSC- and iPSC-nCoVN-derived cardiomyocytes. The cell nuclei were stained by DAPI
338 (blue). The scale bar represents 50 μ m. (C) The cardiac differentiation efficiency of iPSC and iPSC-
339 nCoVN. Images taken from (B) were analyzed by using ImageJ software. The efficiency was
340 calculated as the portion of cardiac Troponin T positive cells in all the cells. Approximately 6,000
341 cells were counted in each group. **, $p<0.001$.

342 **Figure 4.** Long-term expression of nCoVN turned iPSC to fibroblast. (A-C) Representative
343 immunofluorescent staining images of vimentin (green), S100A4 (green), and α -SMA (green) in
344 iPSC-nCoVN after a 10-day induction. The cell nuclei were stained by DAPI (blue). The scale bars
345 represent 10 μ m. (D) The representative bright field image of cells after a 40-day nCoVN expression.
346 The morphology exhibits typical fibroblast features. The scale bar represents 50 μ m. (E) The two
347 most significantly enriched pathways in the down-regulated genes. The histogram shows the
348 significance of the two pathways by using $-\log_{10}(q)$ values with Bonferroni correction. The Log 2-
349 fold change values of a total of 14 genes in these two pathways were exhibited by the heatmap. (F)
350 The three most significantly enriched pathways in the up-regulated genes. The histogram shows the
351 significance of the three pathways by using $-\log_{10}(q)$ values with Bonferroni correction. The Log 2-
352 fold change values of the top 20 up-regulated genes in these pathways were exhibited by the
353 heatmap. (G) The heatmap of the correlation coefficients among iPSC-GFP, iPSC-nCoVN,
354 ESC/iPSC and fibroblast from the ENCODE project. The 1000 most variable genes in the samples
355 were used to calculate the correlation coefficients. iPSC-GFP and iPSC-nCoVN clustered with
356 pluripotent stem cell and fibroblast, respectively.

357 10 References

358 Abujarour, R., Valamehr, B., Robinson, M., Rezner, B., Vraneanu, F., and Flynn, P. (2013).
359 Optimized surface markers for the prospective isolation of high-quality hiPSCs using flow
360 cytometry selection. *Sci Rep* 3, 1179. doi: 10.1038/srep01179.

361 Bernstein, P., Sticht, C., Jacobi, A., Liebers, C., Manthey, S., and Stiehler, M. (2010). Expression
362 pattern differences between osteoarthritic chondrocytes and mesenchymal stem cells during
363 chondrogenic differentiation. *Osteoarthritis Cartilage* 18(12), 1596-1607. doi:
364 10.1016/j.joca.2010.09.007.

365 Bolstad, B.M., Irizarry, R.A., Astrand, M., and Speed, T.P. (2003). A comparison of normalization
366 methods for high density oligonucleotide array data based on variance and bias.
367 *Bioinformatics* 19(2), 185-193. doi: 10.1093/bioinformatics/19.2.185.

368 Bray, N.L., Pimentel, H., Melsted, P., and Pachter, L. (2016). Near-optimal probabilistic RNA-seq
369 quantification. *Nat Biotechnol* 34(5), 525-527. doi: 10.1038/nbt.3519.

370 Chang, C.K., Hou, M.H., Chang, C.F., Hsiao, C.D., and Huang, T.H. (2014). The SARS coronavirus
371 nucleocapsid protein--forms and functions. *Antiviral Res* 103, 39-50. doi:
372 10.1016/j.antiviral.2013.12.009.

373 Chang, C.K., Lo, S.C., Wang, Y.S., and Hou, M.H. (2016). Recent insights into the development of
374 therapeutics against coronavirus diseases by targeting N protein. *Drug Discov Today* 21(4),
375 562-572. doi: 10.1016/j.drudis.2015.11.015.

376 Chen, J., Bardes, E.E., Aronow, B.J., and Jegga, A.G. (2009). ToppGene Suite for gene list
377 enrichment analysis and candidate gene prioritization. *Nucleic Acids Res* 37(Web Server
378 issue), W305-311. doi: 10.1093/nar/gkp427.

379 Cheung, Y.K., Cheng, S.C., Sin, F.W., Chan, K.T., and Xie, Y. (2008). Investigation of
380 immunogenic T-cell epitopes in SARS virus nucleocapsid protein and their role in the
381 prevention and treatment of SARS infection. *Hong Kong Med J* 14 Suppl 4, 27-30.

382 Chinese, S.M.E.C. (2004). Molecular evolution of the SARS coronavirus during the course of the
383 SARS epidemic in China. *Science* 303(5664), 1666-1669. doi: 10.1126/science.1092002.

384 Consortium, E.P. (2012). An integrated encyclopedia of DNA elements in the human genome.
385 *Nature* 489(7414), 57-74. doi: 10.1038/nature11247.

386 Das, D., Kammila, S., and Suresh, M.R. (2010). Development, characterization, and application of
387 monoclonal antibodies against severe acute respiratory syndrome coronavirus nucleocapsid
388 protein. *Clin Vaccine Immunol* 17(12), 2033-2036. doi: 10.1128/CVI.00293-10.

389 Davis, C.A., Hitz, B.C., Sloan, C.A., Chan, E.T., Davidson, J.M., Gabdank, I., et al. (2018). The
390 Encyclopedia of DNA elements (ENCODE): data portal update. *Nucleic Acids Res* 46(D1),
391 D794-D801. doi: 10.1093/nar/gkx1081.

392 Frankish, A., Diekhans, M., Ferreira, A.M., Johnson, R., Jungreis, I., Loveland, J., et al. (2019).
393 GENCODE reference annotation for the human and mouse genomes. *Nucleic Acids Res*
394 47(D1), D766-D773. doi: 10.1093/nar/gky955.

395 He, R., Leeson, A., Andonov, A., Li, Y., Bastien, N., Cao, J., et al. (2003). Activation of AP-1 signal
396 transduction pathway by SARS coronavirus nucleocapsid protein. *Biochem Biophys Res
397 Commun* 311(4), 870-876. doi: 10.1016/j.bbrc.2003.10.075.

398 Hoffmann, M., Kleine-Weber, H., Schroeder, S., Kruger, N., Herrler, T., Erichsen, S., et al. (2020).
399 SARS-CoV-2 Cell Entry Depends on ACE2 and TMPRSS2 and Is Blocked by a Clinically
400 Proven Protease Inhibitor. *Cell*. doi: 10.1016/j.cell.2020.02.052.

401 Hu, Y., Li, W., Gao, T., Cui, Y., Jin, Y., Li, P., et al. (2017). The Severe Acute Respiratory
402 Syndrome Coronavirus Nucleocapsid Inhibits Type I Interferon Production by Interfering
403 with TRIM25-Mediated RIG-I Ubiquitination. *J Virol* 91(8). doi: 10.1128/JVI.02143-16.

404 Jiang, W., Hua, R., Wei, M., Li, C., Qiu, Z., Yang, X., et al. (2015). An optimized method for high-
405 titer lentivirus preparations without ultracentrifugation. *Sci Rep* 5, 13875. doi:
406 10.1038/srep13875.

407 Johnson, W.E., Li, C., and Rabinovic, A. (2007). Adjusting batch effects in microarray expression
408 data using empirical Bayes methods. *Biostatistics* 8(1), 118-127. doi:
409 10.1093/biostatistics/kxj037.

410 Kim, J.J., Khalid, O., Namazi, A., Tu, T.G., Elie, O., Lee, C., et al. (2014). Discovery of consensus
411 gene signature and intermodular connectivity defining self-renewal of human embryonic stem
412 cells. *Stem Cells* 32(6), 1468-1479. doi: 10.1002/stem.1675.

413 Lin, B., Lin, X., Stachel, M., Wang, E., Luo, Y., Lader, J., et al. (2017). Culture in Glucose-Depleted
414 Medium Supplemented with Fatty Acid and 3,3',5-Triiodo-1-Thyronine Facilitates
415 Purification and Maturation of Human Pluripotent Stem Cell-Derived Cardiomyocytes. *Front
416 Endocrinol (Lausanne)* 8, 253. doi: 10.3389/fendo.2017.00253.

417 Love, M.I., Huber, W., and Anders, S. (2014). Moderated estimation of fold change and dispersion
418 for RNA-seq data with DESeq2. *Genome Biol* 15(12), 550. doi: 10.1186/s13059-014-0550-8.

419 Lu, R., Zhao, X., Li, J., Niu, P., Yang, B., Wu, H., et al. (2020). Genomic characterisation and
420 epidemiology of 2019 novel coronavirus: implications for virus origins and receptor binding.
421 *Lancet* 395(10224), 565-574. doi: 10.1016/S0140-6736(20)30251-8.

422 McBride, R., van Zyl, M., and Fielding, B.C. (2014). The coronavirus nucleocapsid is a
423 multifunctional protein. *Viruses* 6(8), 2991-3018. doi: 10.3390/v6082991.

424 Onate, B., Vilahur, G., Camino-Lopez, S., Diez-Caballero, A., Ballesta-Lopez, C., Ybarra, J., et al.
425 (2013). Stem cells isolated from adipose tissue of obese patients show changes in their
426 transcriptomic profile that indicate loss in stemcellness and increased commitment to an
427 adipocyte-like phenotype. *BMC Genomics* 14, 625. doi: 10.1186/1471-2164-14-625.

428 Pang, W.W., Price, E.A., Sahoo, D., Beerman, I., Maloney, W.J., Rossi, D.J., et al. (2011). Human
429 bone marrow hematopoietic stem cells are increased in frequency and myeloid-biased with
430 age. *Proc Natl Acad Sci U S A* 108(50), 20012-20017. doi: 10.1073/pnas.1116110108.

431 Rowland, R.R., Chauhan, V., Fang, Y., Pekosz, A., Kerrigan, M., and Burton, M.D. (2005).
432 Intracellular localization of the severe acute respiratory syndrome coronavirus nucleocapsid
433 protein: absence of nucleolar accumulation during infection and after expression as a
434 recombinant protein in vero cells. *J Virol* 79(17), 11507-11512. doi:
435 10.1128/JVI.79.17.11507-11512.2005.

436 Severance, E.G., Bossis, I., Dickerson, F.B., Stallings, C.R., Origoni, A.E., Sullens, A., et al. (2008).
437 Development of a nucleocapsid-based human coronavirus immunoassay and estimates of
438 individuals exposed to coronavirus in a U.S. metropolitan population. *Clin Vaccine Immunol*
439 15(12), 1805-1810. doi: 10.1128/CVI.00124-08.

440 Shalem, O., Sanjana, N.E., Hartenian, E., Shi, X., Scott, D.A., Mikkelsen, T., et al. (2014). Genome-
441 scale CRISPR-Cas9 knockout screening in human cells. *Science* 343(6166), 84-87. doi:
442 10.1126/science.1247005.

443 Shekhar, A., Lin, X., Lin, B., Liu, F.Y., Zhang, J., Khodadadi-Jamayran, A., et al. (2018). ETV1
444 activates a rapid conduction transcriptional program in rodent and human cardiomyocytes. *Sci
445 Rep* 8(1), 9944. doi: 10.1038/s41598-018-28239-7.

446 Song, Z., Xu, Y., Bao, L., Zhang, L., Yu, P., Qu, Y., et al. (2019). From SARS to MERS, Thrusting
447 Coronaviruses into the Spotlight. *Viruses* 11(1). doi: 10.3390/v11010059.

448 Suresh, M.R., Bhatnagar, P.K., and Das, D. (2008). Molecular targets for diagnostics and
449 therapeutics of severe acute respiratory syndrome (SARS-CoV). *J Pharm Pharm Sci* 11(2),
450 1s-13s. doi: 10.18433/j3j019.

451 Surjit, M., Liu, B., Jameel, S., Chow, V.T., and Lal, S.K. (2004). The SARS coronavirus
452 nucleocapsid protein induces actin reorganization and apoptosis in COS-1 cells in the absence
453 of growth factors. *Biochem J* 383(Pt 1), 13-18. doi: 10.1042/BJ20040984.

454 Trusler, O., Huang, Z., Goodwin, J., and Laslett, A.L. (2018). Cell surface markers for the
455 identification and study of human naive pluripotent stem cells. *Stem Cell Res* 26, 36-43. doi:
456 10.1016/j.scr.2017.11.017.

457 Wrapp, D., Wang, N., Corbett, K.S., Goldsmith, J.A., Hsieh, C.L., Abiona, O., et al. (2020). Cryo-
458 EM structure of the 2019-nCoV spike in the prefusion conformation. *Science* 367(6483),
459 1260-1263. doi: 10.1126/science.abb2507.

460 Wu, A., Peng, Y., Huang, B., Ding, X., Wang, X., Niu, P., et al. (2020). Genome Composition and
461 Divergence of the Novel Coronavirus (2019-nCoV) Originating in China. *Cell Host Microbe*
462 27(3), 325-328. doi: 10.1016/j.chom.2020.02.001.

463 Xu, X., P., C., J., W., J., F., H., Z., X., L., et al. (2020). Evolution of the novel coronavirus from the
464 ongoing Wuhan outbreak and modeling of its spike protein for risk of human transmission.
465 *Sci China Life Sci* 63. doi: <https://doi.org/10.1007/s11427-020-1637-5>.

466 Yang, R., Zheng, Y., Burrows, M., Liu, S., Wei, Z., Nace, A., et al. (2014). Generation of
467 folliculogenic human epithelial stem cells from induced pluripotent stem cells. *Nat Commun*
468 5, 3071. doi: 10.1038/ncomms4071.

469 Zhang, L., Wei, L., Jiang, D., Wang, J., Cong, X., and Fei, R. (2007a). SARS-CoV nucleocapsid
470 protein induced apoptosis of COS-1 mediated by the mitochondrial pathway. *Artif Cells
471 Blood Substit Immobil Biotechnol* 35(2), 237-253. doi: 10.1080/10731190601188422.

472 Zhang, X., Wu, K., Wang, D., Yue, X., Song, D., Zhu, Y., et al. (2007b). Nucleocapsid protein of
473 SARS-CoV activates interleukin-6 expression through cellular transcription factor NF-
474 kappaB. *Virology* 365(2), 324-335. doi: 10.1016/j.virol.2007.04.009.

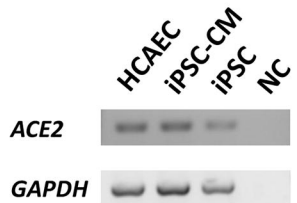
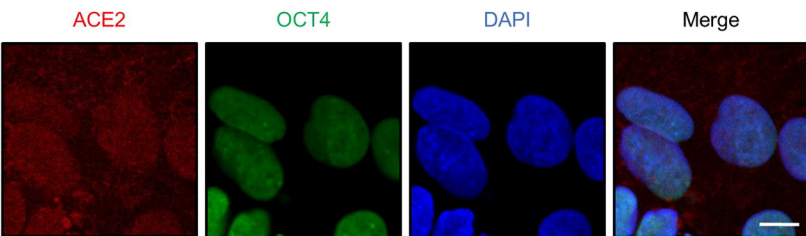
475 Zhao, G., Shi, S.Q., Yang, Y., and Peng, J.P. (2006). M and N proteins of SARS coronavirus induce
476 apoptosis in HPF cells. *Cell Biol Toxicol* 22(5), 313-322. doi: 10.1007/s10565-006-0077-1.

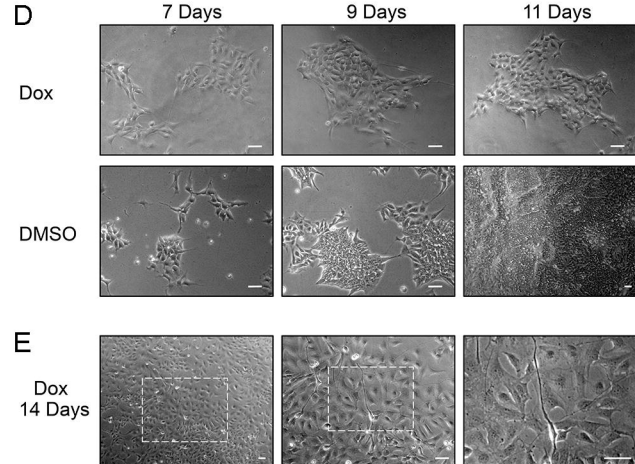
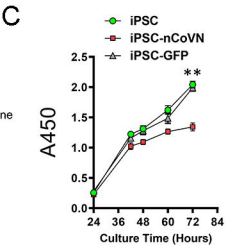
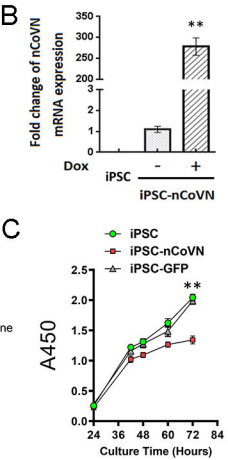
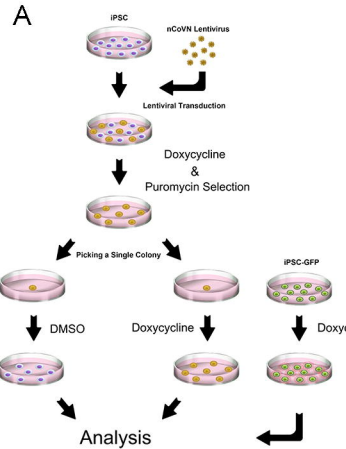
477 Zhao, X., Nicholls, J.M., and Chen, Y.G. (2008). Severe acute respiratory syndrome-associated
478 coronavirus nucleocapsid protein interacts with Smad3 and modulates transforming growth
479 factor-beta signaling. *J Biol Chem* 283(6), 3272-3280. doi: 10.1074/jbc.M708033200.

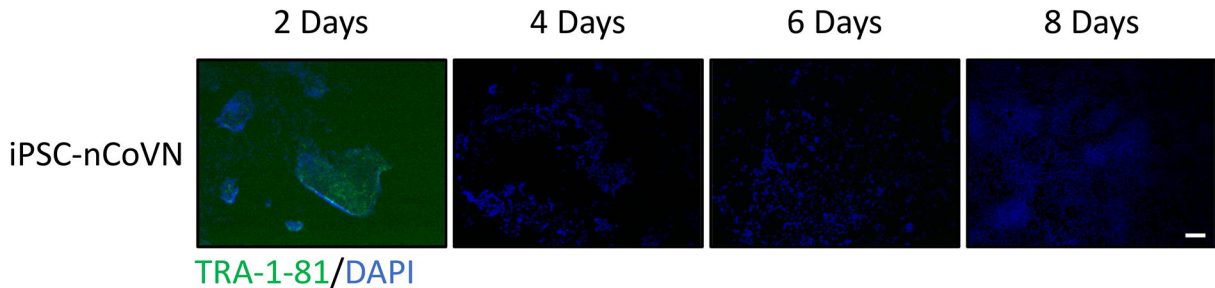
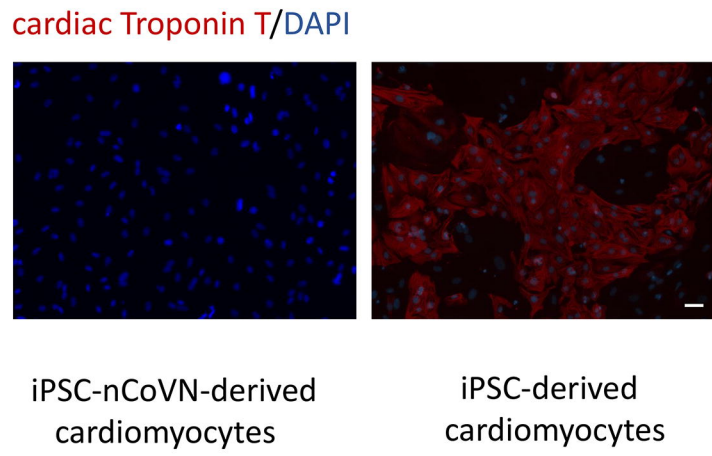
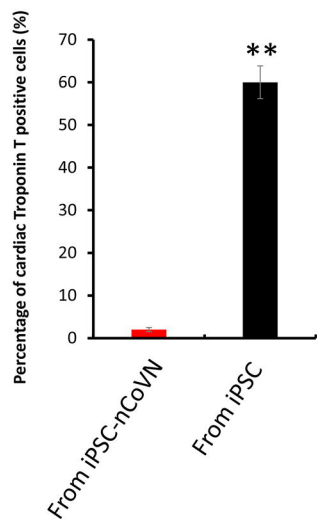
480 Zhou, B., Liu, J., Wang, Q., Liu, X., Li, X., Li, P., et al. (2008). The nucleocapsid protein of severe
481 acute respiratory syndrome coronavirus inhibits cell cytokinesis and proliferation by
482 interacting with translation elongation factor 1alpha. *J Virol* 82(14), 6962-6971. doi:
483 10.1128/JVI.00133-08.

A

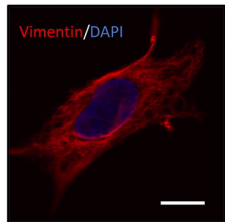
Dataset	Sample	Cell Line	ACE2 Ave Value	GAPDH Ave Value
GDS5408	GSM1309417	human embryonic stem cell H1 1	25.61	24162.72
	GSM1309418	human embryonic stem cell H1 2	30.16	26123.47
	GSM1309421	human embryonic stem cell H9 1	39.93	24325.00
	GSM1309422	human embryonic stem cell H9 2	27.90	23177.18
GDS5638	GSM1235179	human induced pluripotent stem cell 1	62.92	29904.83
	GSM1235180	human induced pluripotent stem cell 2	76.38	30926.80
	GSM1235184	human epithelial stem cell 1	67.86	15493.84
	GSM1235185	human epithelial stem cell 2	70.71	23540.97
GDS5056	GSM1187676	human adipose stem cell 1	5.77	14.29
	GSM1187677	human adipose stem cell 2	5.72	14.31
	GSM1187678	human adipose stem cell 3	5.87	14.34
GDS3942	GSM812988	human hematopoietic stem cell 1	3.77	12.47
	GSM812989	human hematopoietic stem cell 2	4.71	12.54
	GSM812990	human hematopoietic stem cell 3	4.20	12.61
GDS3785	GSM490983	human mesenchymal stem cell	5.47	12.29

B**C**

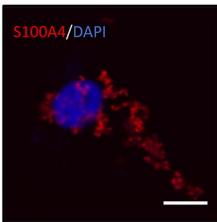


A**B****C**

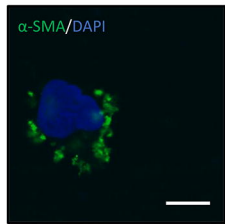
A



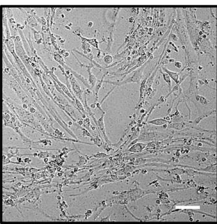
B



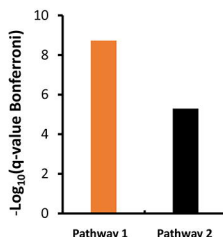
C



D



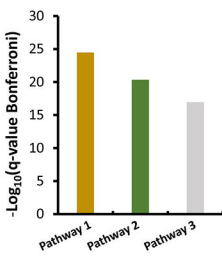
E



POU5F1 (OCT4), SOX2, NANOG activate genes related to proliferation

Transcriptional regulation of pluripotent stem cells

F



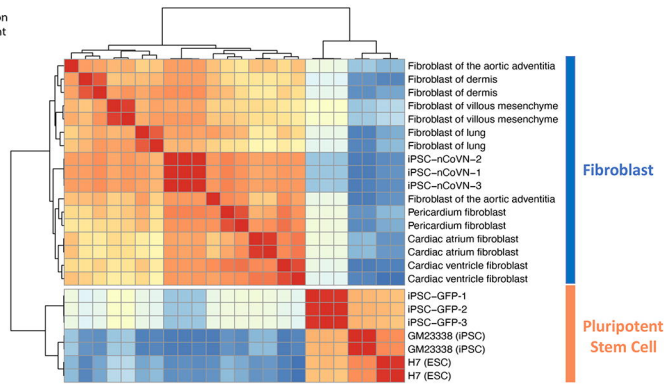
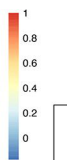
Extracellular matrix and extracellular matrix-associated proteins

Core extracellular matrix (ECM glycoproteins, collagens and proteoglycans)

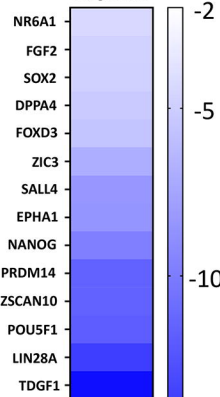
Extracellular matrix organization

G

Correlation Coefficient



Genes Log 2-fold change values



Genes Log 2-fold change values

